Supporting information for:

Bacterial inactivation by a carbon nanotube-iron oxide nanocomposite: A mechanistic study using *E. coli* mutants

Maya Engel [1], Yitzhak Hadar [2], Shimshon Belkin [3], Xinglin Lu [4], Menachem Elimelech [4] and Benny Chefetz [*, 1]

[1] Department of Soil and Water Sciences, Faculty of Agriculture, Food and Environment, The Hebrew University of Jerusalem, Rehovot 7610001, Israel

[2] Department of Plant Pathology and Microbiology, Faculty of Agriculture, Food and Environment, The Hebrew University of Jerusalem, Rehovot 7610001, Israel

[3] Department of Plant and Environmental Sciences, Institute of Life Sciences, The Hebrew University of Jerusalem, Jerusalem 91904, Israel

[4] Department of Chemical and Environmental Engineering, Yale University, New Haven, Connecticut 06520-8286, United States

[*]Corresponding author: Benny Chefetz
E-mail: benny.chefetz@mail.huji.ac.il
Tel.: 972-8-9489384; fax: 972-8-9475181

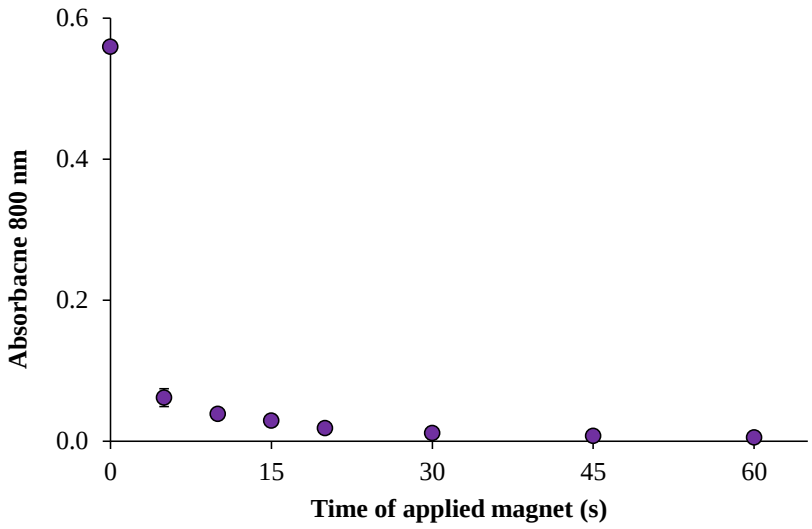

Figure S1. Magnetic separation of the single-walled carbon nanotube-iron oxide nanocomposite material from solution, monitored at 800 nm.

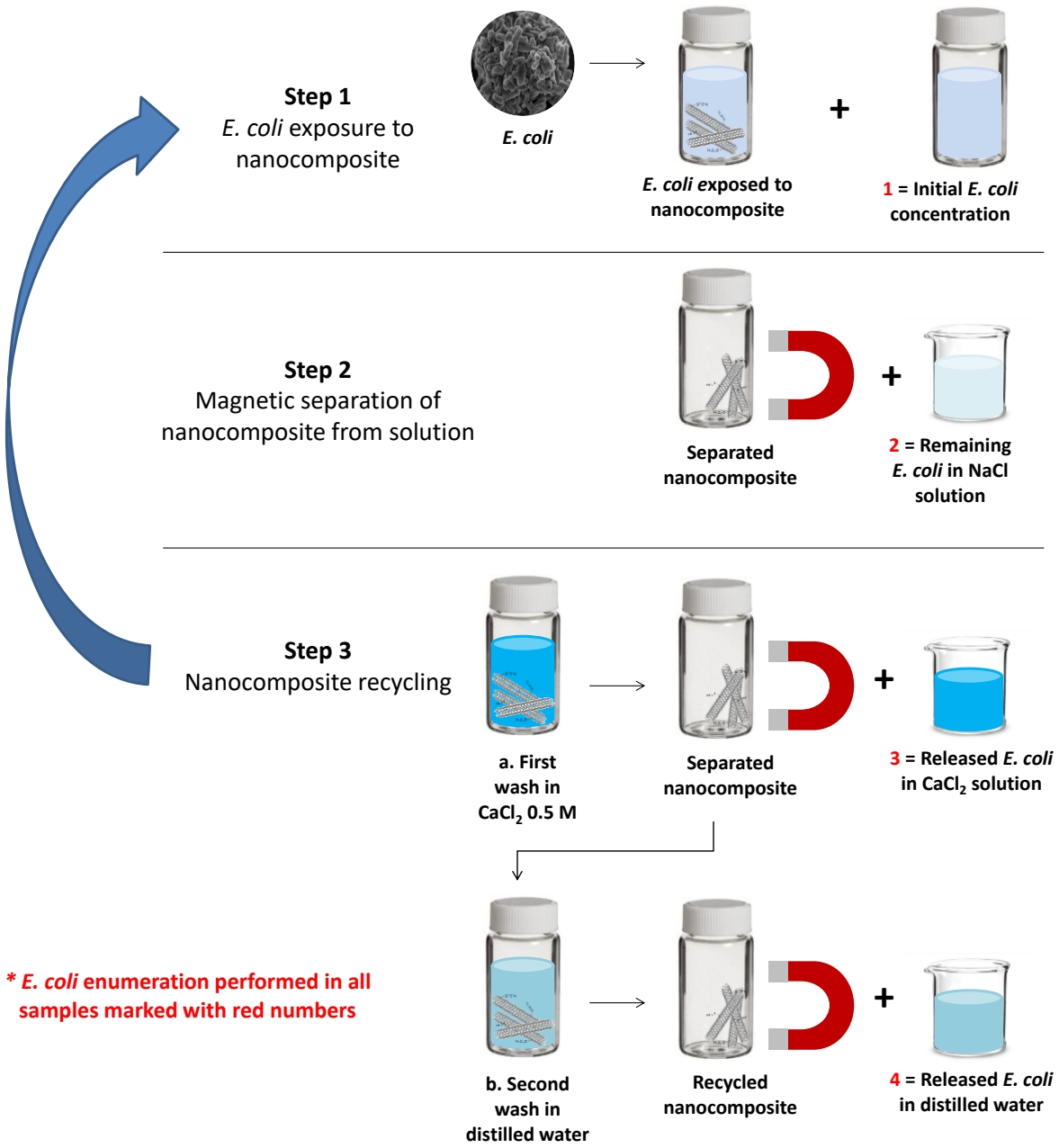

Figure S2. Schematic diagram of nanocomposite exposure and recycling (scheme illustrates one entire cycle).

Material characterization

The morphologies and sizes of the single-walled carbon nanotubes (SWCNTs), iron oxide nanoparticles (NPs) and SWCNT-iron oxide nanocomposite are presented in Figure S3. The iron oxide NPs are generally spherical with diameters ranging between 3 to 40 nm. The nanocomposite material unveils an intertwined network of SWCNTs embedded with clusters of iron oxide nanoparticles (diameters ranging between 5 to 60 nm). The surface area, mesopore, and micropore volumes of the nanocomposite material decreased in comparison to the SWCNTs from 443 to 240 m^2 g^{-1}, 1.1 to 0.71 cm^3 g^{-1} and 0.22 to 0.12 cm^3 g^{-1}, respectively. Thermal gravimetric analysis of the bare SWCNTs, iron oxide NPs and SWCNT-iron oxide nanocomposite material recorded mass losses of 86 ± 8%, 2 ± 1% and 37 ± 4%, respectively (representative thermograms are shown in Figure S4). This indicates that the purity of the iron oxide NPs is 98% and that the mass percentage of iron oxide in the nanocomposite material is 63 ± 4%. In accordance, elemental analysis revealed the mass carbon percentage in the nanocomposite as 38 ± 1%.

The broad band at ~3380 cm^{-1} in the FTIR spectra of the iron oxide NPs and SWCNT-iron oxide nanocomposite material is attributed to the O–H stretching vibration originating from surface hydroxyl groups (Figure S5). In the iron oxide-SWCNT nanocomposite material spectrum the two peaks at 1630 and 1589 cm^{-1} may be assigned to C=O and C=C stretching, respectively. Moreover, the stretching vibration of C–O is observed at 1383 and 1052 cm^{-1}. The peak at ~570 cm^{-1} in the spectra of the iron oxide NPs and iron oxide-SWCNT nanocomposite material is ascribed to the vibration of Fe–O in magnetite.[1–3] However, the additional peak at 632 cm^{-1} in the iron oxide spectrum likely arises from the presence of maghemite.[4] The X-ray diffractograms of the SWCNTs, iron oxide NPs and SWCNT-iron oxide

nanocomposite material demonstrate the co-existence of SWCNTs and iron oxides in the nanocomposite (Figure S6). The peaks at 2θ=30.2°, 35.5°, 53.5°, 57.2° and 62.9° are characteristic of magnetite and/or maghemite[2,5,6] whereas the peak at 2θ=26.4° is related to the SWCNTs. The peak at 43.2° may be ascribed to both the SWCNTs and the iron oxide NPs. Figure S7 exhibits the deconvoluted X-ray electron spectra of Fe 2p for the iron oxide NPs and iron oxide SWCNT nanocomposite. The peaks of Fe 2p1/2 and Fe 2p3/2 found at 710.9 and 724.5 eV in the spectrum of the iron oxide NPs and at 711.2 and 724.6 eV in the spectrum of the nanocomposite are indicative of a mixture of magnetite and maghemite, respectively. Moreover, a satellite peak at ~719 eV is typical of maghemite.[3,7,8] The O/Fe and C/O/Fe atomic ratios are 2.9:1.0 and 8.5:3.2:1.0 in the iron oxide and iron oxide-SWCNT nanocomposite material, respectively.

The magnetic properties of the iron oxide NPs and iron oxide-SWCNT nanocomposite material are presented in Figure S8. The magnetization saturation of the iron oxide NPs and the nanocomposite material were 126.7 and 40.71 emu g^{-1}, respectively, similar to values reported in additional studies.[1,5,9] The facile magnetic separation of the nanocomposite material is illustrated in the photograph (Figure S8).

REFERENCES

1 J. Hu, D. Shao, C. Chen, G. Sheng, J. Li, X. Wang and M. Nagatsu, *J. Phys. Chem. B*, 2010, **114**, 6779–6785.

2 L. Ai, C. Zhang, F. Liao, Y. Wang, M. Li, L. Meng and J. Jiang, *J. Hazard. Mater.*, 2011, **198**, 282–290.

3 X. Yang, C. Chen, J. Li, G. Zhao, X. Ren and X. Wang, *RSC Adv.*, 2012, **2**, 8821–8826.

4 E. Darezereshki, *Mater. Lett.*, 2010, **64**, 1471–1472.

5 C. L. Chen, X. K. Wang and M. Nagatsu, *Environ. Sci. Technol.*, 2009, **43**,

2362–2367.

6 M. A. Legodi and D. De Waal, *Dye. Pigment.*, 2006, **74**, 161–168.

7 T. Yamashita and P. Hayes, *Appl. Surf. Sci.*, 2008, **254**, 2441–2449.

8 J. Lu, X. Jiao, D. Chen and W. Li, *J. Phys. Chem. C*, 2009, **113**, 4012–4017.

9 X. Zhang, J. Qian and B. Pan, *Environ. Sci. Technol.*, 2015, **50**, 881–889.

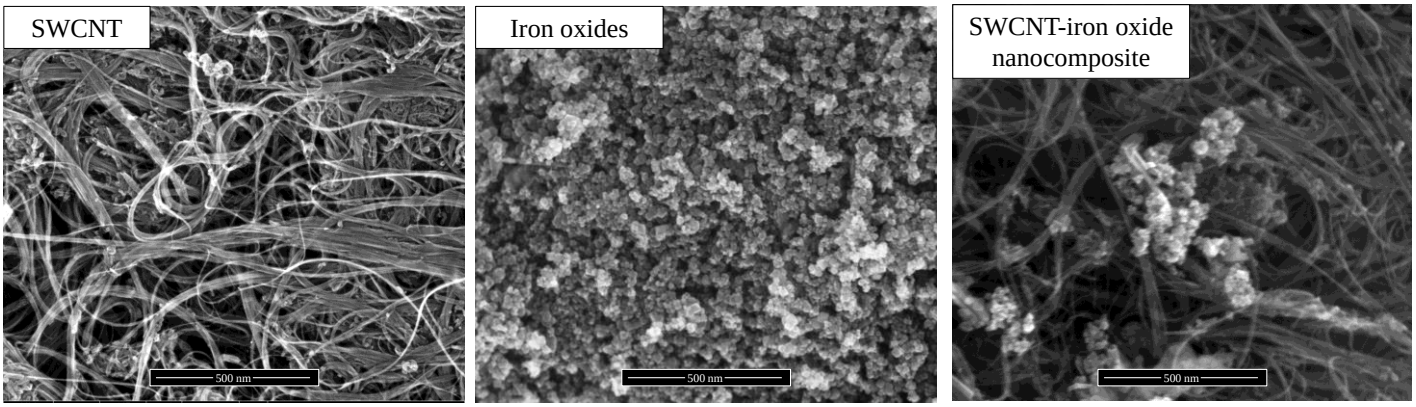

Figure S3. Scanning electron microscopy images of single walled carbon nanotubes (SWCNTs), iron oxide nanoparticles and the SWCNT-iron oxide nanocomposite.

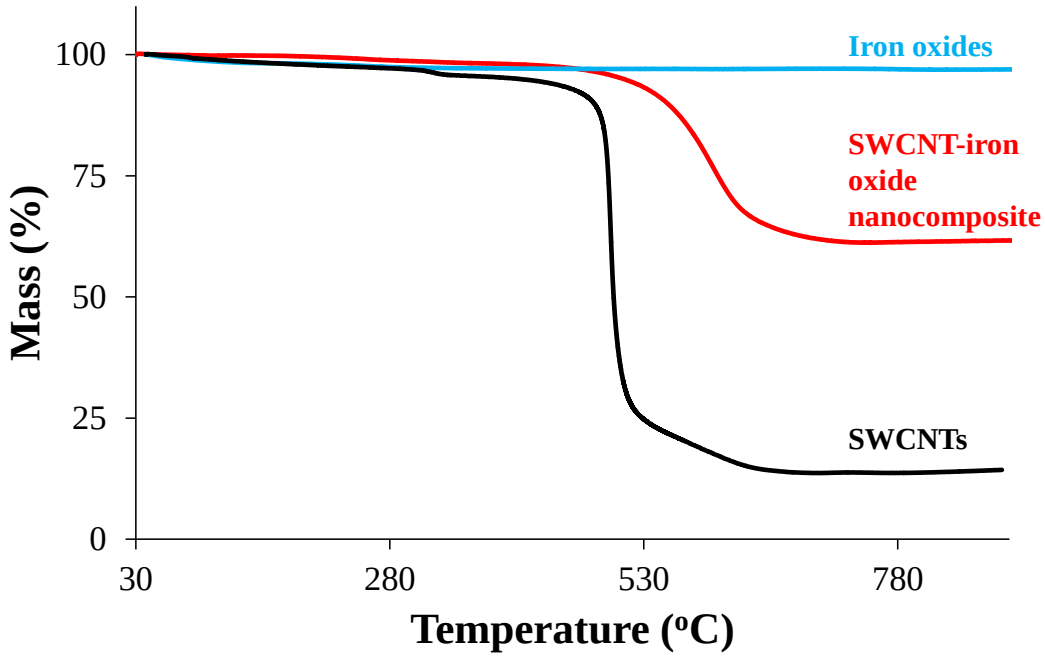

Figure S4. Representative thermograms of the iron oxide nanoparticles, single-walled carbon nanotubes (SWCNTs) and SWCNT-iron oxide nanocomposite.

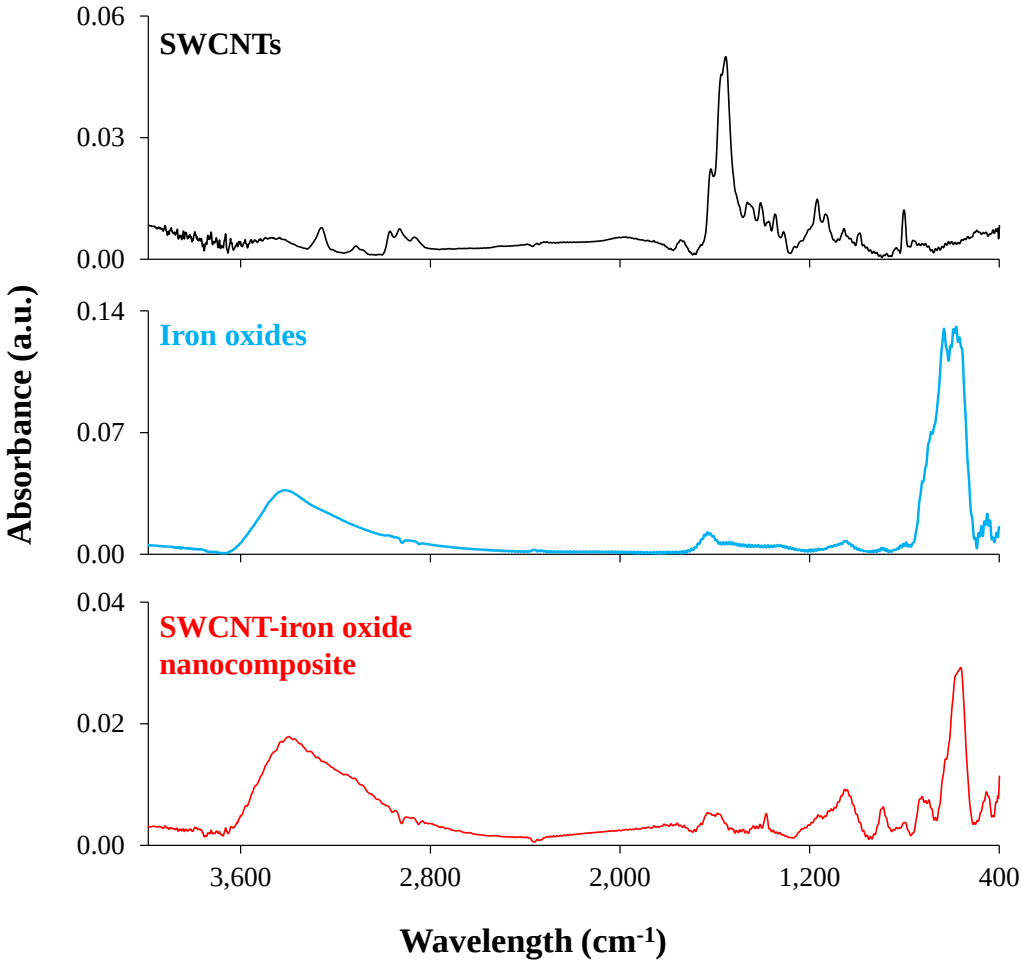

Figure S5. Fourier transform infrared spectra of the single-walled carbon nanotubes (SWCNTs), iron oxide nanoparticles and the SWCNT-iron oxide nanocomposite.

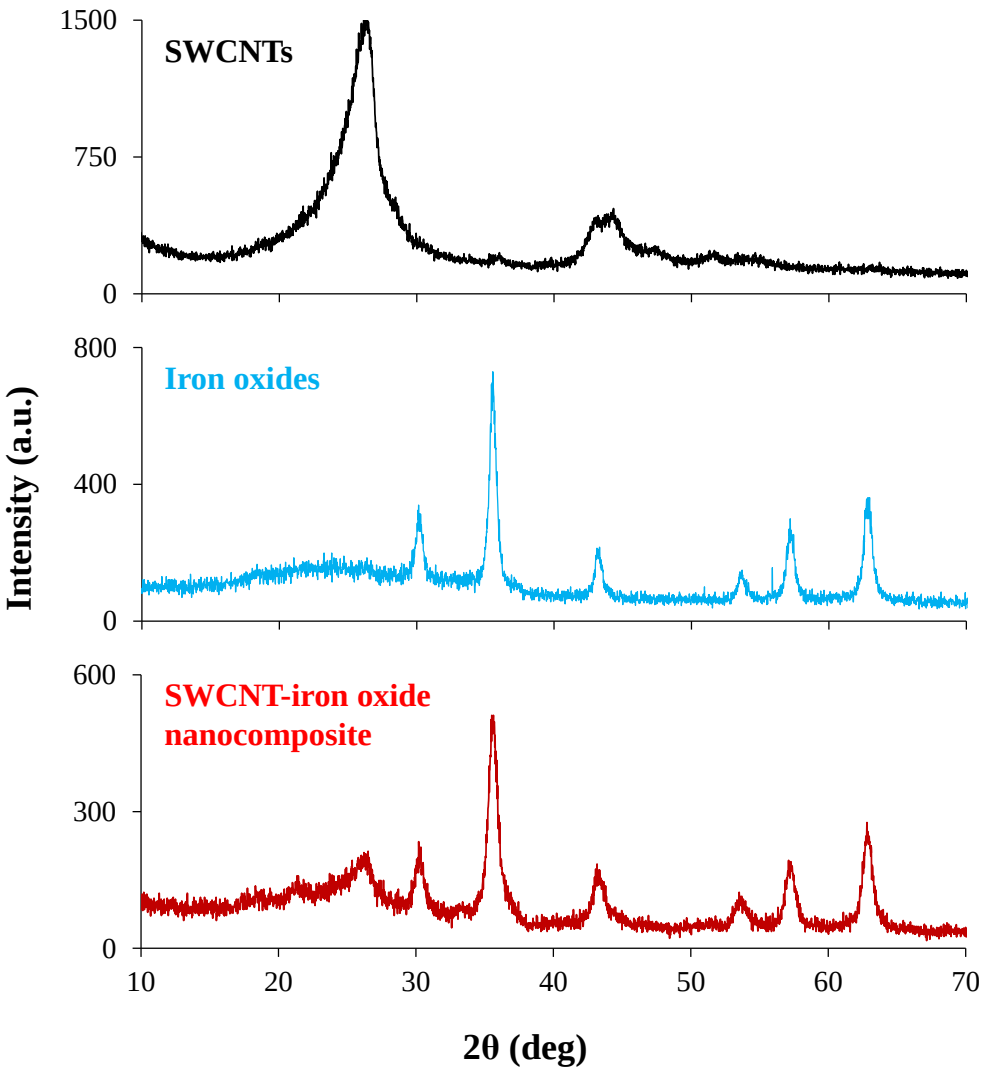

Figure S6. X-ray diffractograms of the single-walled carbon nanotubes (SWCNTs), iron oxide nanoparticles and the SWCNT-iron oxide nanocomposite.

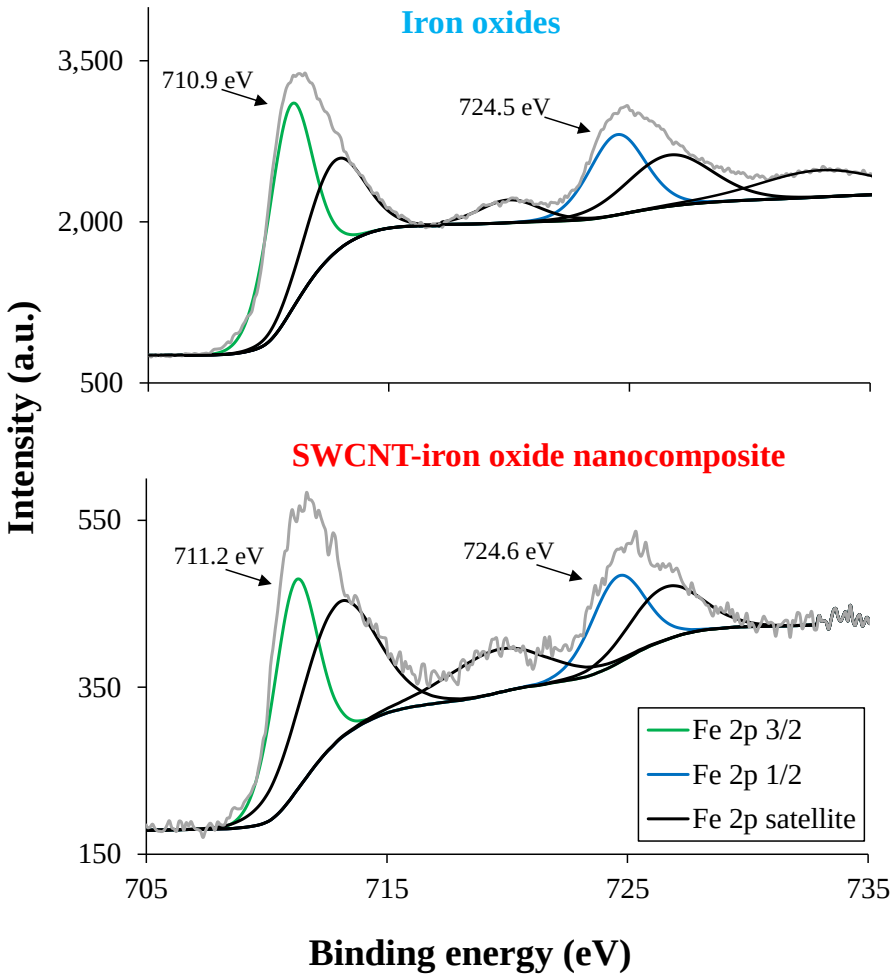

Figure S7. Deconvoluted X-ray electron spectra of Fe 2p for the iron oxide nanoparticles and single-walled carbon nanotube (SWCNT)-iron oxide nanocomposite.

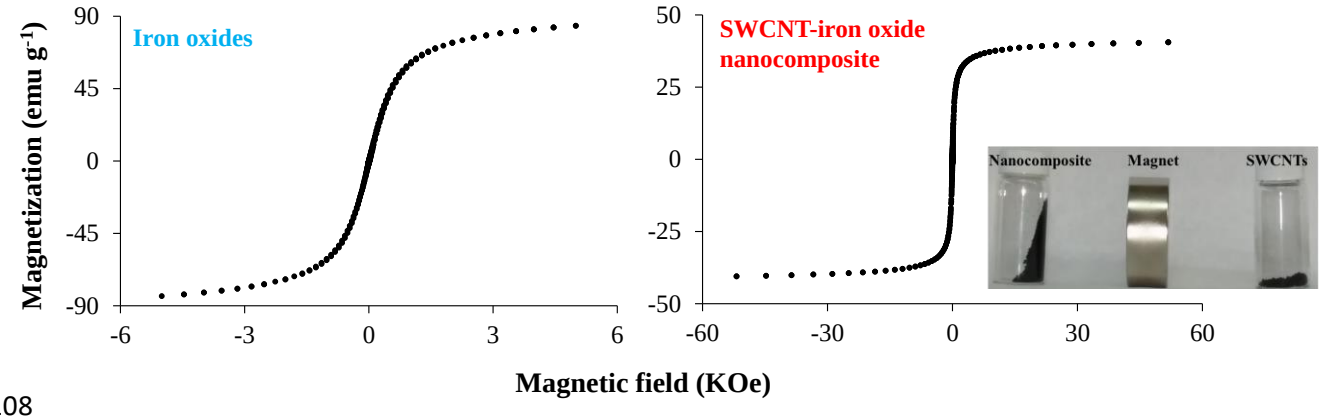

Figure S8. Magnetization curves of the iron oxide nanoparticles and single-walled carbon nanotube (SWCNT)-iron oxide nanocomposite. In the photograph: magnetic separation of the nanocomposite (left) compared to the bare SWCNTs (right).

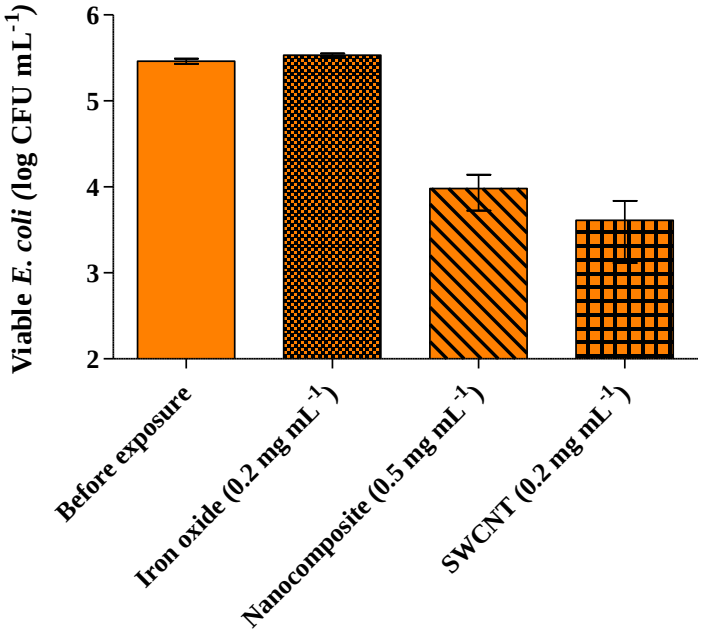

Figure S9. Levels of live *E. coli* (MG1655) in solution before and after exposure to the single-walled carbon nanotube (SWCNT)-iron oxide nanocomposite, iron oxide nanoparticles and pristine SWCNTs.

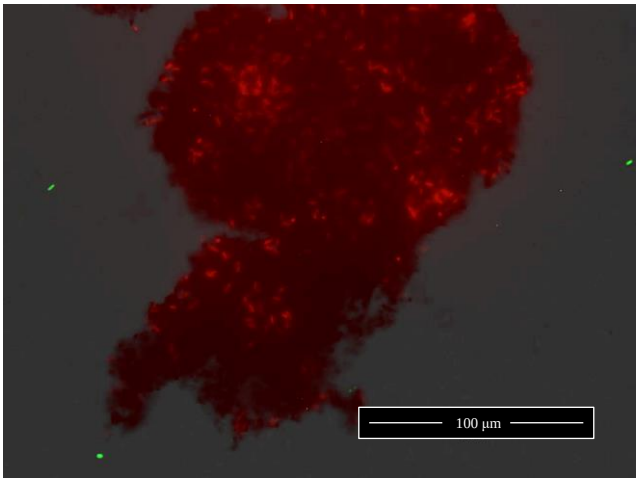

Figure S10. Representative fluorescence microscopy imaging of the single-walled carbon nanotube-iron oxide nanocomposite following interaction with the BW25113 Δ*rfaC* strain. Live and dead cells appear in green and red, respectively.

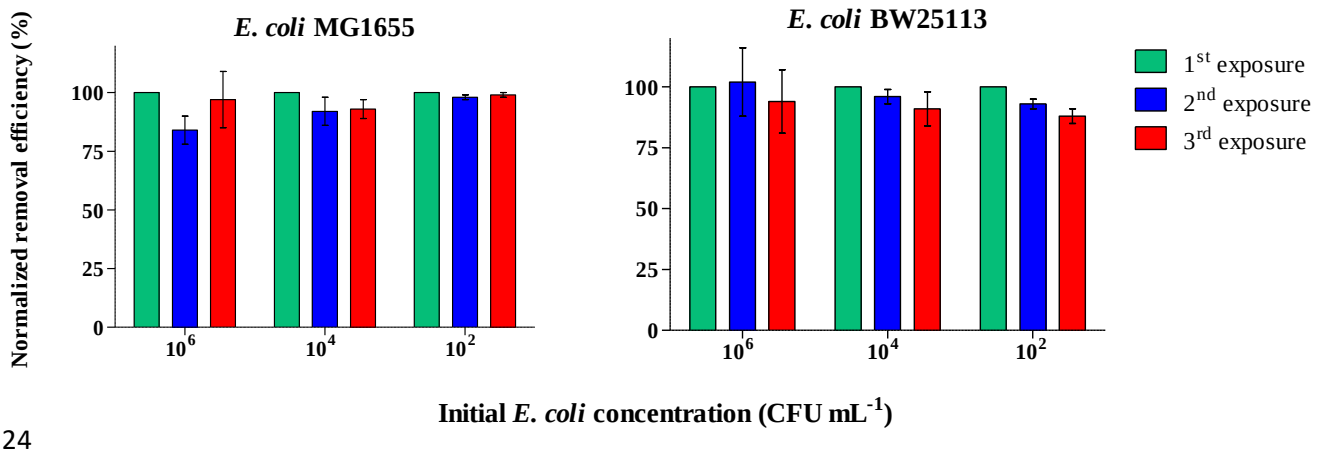

Figure S11. Removal efficiency of *E. coli* by the single-walled carbon nanotube-iron oxide nanocomposite following three sequential exposure cycles (results normalized to the efficiency of the first exposure cycle).

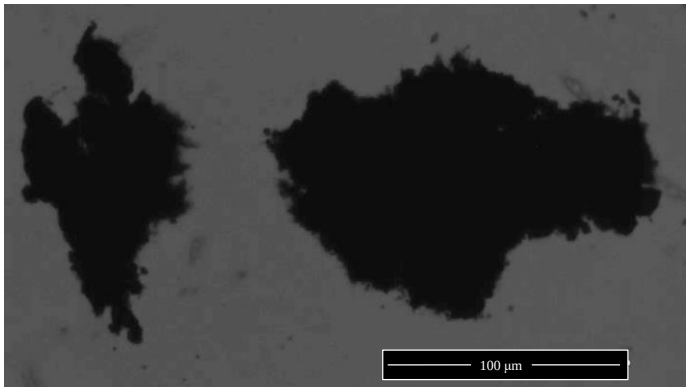

Figure S12. Representative fluorescence microscopy imaging of the single-walled carbon nanotube-iron oxide nanocomposite after the washing procedure (following the first exposure cycle). Live and dead cells appear in green and red, respectively.